Accepted Manuscript

Thermal, electrical, and magnetic properties of Fe_2O_3–PbO–SiO_2 glass prepared by traditional melt-quenching and twin roller fast-cooling methods

A. Lenarciak, N.A. Wójcik, P. Kupracz, J. Strychalska-Nowak, Z. Sobczak, M. Prześniak-Welenc, J. Karczewski, R.J. Barczyński

Please cite this article as: A. Lenarciak, N.A. Wójcik, P. Kupracz, J. Strychalska-Nowak, Z. Sobczak, M. Prześniak-Welenc, J. Karczewski, R.J. Barczyński, Thermal, electrical, and magnetic properties of Fe_2O_3–PbO–SiO_2 glass prepared by traditional melt-quenching and twin roller fast-cooling methods, *Journal of Physics and Chemistry of Solids* (2019), doi: https://doi.org/10.1016/j.jpcs.2019.05.007.

Thermal, electrical, and magnetic properties of Fe_2O_3-PbO-SiO_2 glass prepared by traditional melt-quenching and twin roller fast-cooling methods

A. Lenarciak[1*], N. A. Wójcik[1,2*], P. Kupracz[1,3], J. Strychalska-Nowak[1], Z. Sobczak[1], M. Prześniak-Welenc[1], J. Karczewski[1], R. J. Barczyński[1]

[1] *Department of Solid State Physics, Faculty of Applied Physics and Mathematics, Gdańsk University of Technology, Narutowicza Street 11/12, 80-233 Gdańsk, Poland*

[2] *Department of Built Environment and Energy Technology, Linnæus University, 35195 Växjö, Sweden*

[3] *Centre for Plasma and Laser Engineering, Szewalski Institute of Fluid Flow Machinery, Polish Academy of Science, Fiszera 14, Gdańsk 80-231, Poland*

[*]Corresponding author e-mail: ariel.lenarciak@pg.edu.pl, natalia.wojcik@pg.edu.pl

Abstract

In this study, Fe-Pb-Si oxide glasses containing between 12.5 and 17.5 mol% Fe_2O_3 were prepared using two different methods comprising traditional melt-quenching and twin roller fast-cooling techniques. The topography and structure of the materials obtained were characterized by X-ray powder diffraction and scanning electron microscopy. All of the materials were found to be amorphous. The topography of most of the glasses comprised random or evenly distributed nanostructures, where the size and amount were dependent on the iron content and preparation technique. The thermal properties of the glasses were analyzed by differential scanning calorimetry, which showed that the glass transition temperatures varied between 529°C and 552°C. The electric conductivity and magnetic susceptibility of the glasses were analyzed by impedance spectroscopy and with an alternating current magnetic properties measurement system, respectively. The measurements of the electrical properties indicated a relatively low activation energy for direct current conductivity (~0.5 to 0.68 eV), which is typical of the polaron hopping mechanism. All of the materials exhibited magnetic hysteresis loops and they were ferromagnetic.

1. Introduction

The magnetic properties of glasses containing different transition metal ions (such as Mn, Fe, Ti) have been studied widely [1-10]. The Fe_2O_3-SiO_2-PbO glasses appear to be interesting materials because of their possible ferromagnetic properties and amorphous structures [5, 11]. However, little is known about the magnetic properties of iron-lead-silicate glasses, whereas the magnetic properties of glass-ceramic materials have been investigated in many studies. In particular, there have

been no previous comparisons of the magnetic (coercivity and remanence) and electrical properties of the Fe-Pb-Si-O glass system when prepared using different techniques, including the fast-cooling (FC) method.

In our previous study [5], we investigated the properties of Fe_2O_3-SiO_2-PbO glasses with different Fe_2O_3 contents and ratios of SiO_2 and PbO. These materials were found to contain nanostructures and they exhibited stronger magnetization than the surrounding matrix. Moreover, the Fe-Pb-Si-O glass system had good dielectric properties and these combined with their ferromagnetic properties may make them suitable candidates for applications in electrical devices such as inductor cores, microtransformers, and sensors [12]. In particular, interesting results were obtained for a glass doped with 15 mol% Fe_2O_3, which contained amorphous spherical nanogranules and it exhibited ferromagnetic properties, whereas a glass with 10 mol% was homogenous and that with 20 mol% was partially crystalline. Therefore, in this study we investigate more compositions with Fe_2O_3 contents between 10 and 20 mol% and we determine their magnetic properties what was not done yet. In addition, in 2016, Tavoosi et al. [6] observed a narrow magnetic hysteresis loop in B_2O_3-SiO_2-BaO-Fe_2O_3 glass-ceramic materials prepared with the FC method and they noted that an increase in the amount of Fe_2O_3 caused an increase in coercivity. The possibility of influencing the magnetic hysteresis loop by changing the Fe_2O_3 content and the preparation conditions merits further investigation.

Oxide glasses containing transition metal oxides (such as Fe_2O_3) exhibit electrical conductivity, which is determined by the presence of the transition metal ion in two valence states [11,13-14]. In these materials, the electrical conduction process is mostly due to a polaron hopping mechanism [15]. A polaron is a quasiparticle comprising an electron and lattice distortion (phonon), which move together in the material's structure. The production of polarons confers energy benefits. In 1974, Anderson and MacCrone [16] measured the electrical conductivity of the Fe-Pb-Si-O glass system with a low Fe_2O_3 content (below 10 mol%) in the temperature range between 77 and 700 K, where they determined the dominant conduction mechanism as polaron hopping between iron ions in different valence states and observed an increase in the conductivity as the Fe_2O_3 content increased.

In the present study, we aimed to determine the effects of different cooling techniques on the structure, thermal, electrical, and magnetic properties of iron-lead-silicate glasses. We also investigated the effects of changes in the Fe contents and

2

preparation method on the direct current (DC) conductivity parameters and magnetization.

2. Experimental procedure

Glass samples with nominal compositions of xFe_2O_3-$(50-x)PbO$-$50SiO_2$, where x = 12.5, 15, 17.5 (mol%), were prepared using two methods comprising the conventional melt-quenching (MQ) technique and the twin roller (FC) method. Analytical grade substrates were used: Fe_2O_3, SiO_2, and PbO (POCH S. A.). The appropriate amounts of reagents were mixed in an agate mortar. The powders obtained were melted in porcelain un-enamelled crucibles in an electric furnace at a temperature of 1623 K for 1–2 h. Porcelain crucibles were used instead of platinum crucibles because platinum reacts with lead compounds above 1173 K [17]. Moreover, un-enamelled porcelain crucibles exhibited the highest chemical resistance at the high temperatures required for our melts among all of the crucibles tested. The first series of melts were poured onto a brass plate, which was preheated to 573 K, and pressed with a stamp to obtain flat circular samples designated as MQ samples. The cooling rate to a temperature of 573 K was estimated as less than 1 min (cooling rate ~20 K s^{-1}). The thickness of the MQ glasses was around 1 mm. The second series of melts were dropped into twin rollers rotating at 2000 rpm (linear speed = 5 ms^{-1}). The approximate cooling rate was estimated as ~10^6 Ks^{-1}. Using this method, samples were obtained in the form of thin tapes with thicknesses ranging from 50 to 90 μm. The materials prepared using the FC technique were designated as FC samples.

The amorphous structures in the samples were analyzed with the X-ray diffraction (XRD) method using an X'Pert Pro MPD system with CuKα radiation. The measurements were acquired over a 2θ range of 10–65° at room temperature with powdered samples.

The topography and compositions of the samples were investigated by scanning electron microscopy (SEM) and using an FEI Company Quanta FEG250 system with an energy dispersive X-ray (EDX) spectrometer (EDAX GENESIS Apex Apollo X60). Measurements were conducted using a beam at accelerating voltages of 30 and 10 kV with a detector secondary electron Everhart–Thornley detector working in the high vacuum mode (pressure 10^{-4} Pa). SEM images were collected from fresh cross-sections of MQ samples and the surfaces of FC samples. EDX

3

analysis was conducted to confirm the presence and among of Al, which may have dissolved from the crucible material.

The thermal properties of the glasses were investigated by differential scanning calorimetry (DSC). DSC measurements were obtained up to 1073 K using powdered samples placed in Pt-Rh crucibles with lids under a flow of synthetic air with a Netzsch STA 449F1 instrument and at a heating rate of 15 K min^{-1}. The onset point of endothermic drift in the DSC curve was treated as the glass transition temperature T_g. The parameters of the thermal properties were estimated using the dedicated software Netzsch Proteus-6. The precision of the thermal process temperature determinations depended on the temperature range selected and it varied by up to ± 2% from the determined value.

The electrical properties were investigated using a Novocontrol Concept 40 broadband dielectric spectrometer. Alternating current (AC) electrical measurements were obtained in the temperature range from 153 K to 423 K in the frequency range from 10 mHz to 1 MHz and at an AC voltage of 1 V_{rms}. To acquire the electrical measurements, gold electrodes were evaporated onto the basal surfaces of previously polished glass samples prepared by the conventional MQ method. The FC samples were broken easily, and thus the gold electrodes were evaporated onto their unpolished surfaces.

The DC magnetic susceptibility was measured as functions of the magnetic field and temperature using a Quantum Design Physical Property Measurement System (PPMS) with the Susceptibility Option (ACMS). Magnetic hysteresis loops were measured at a temperature of 300 K and in the magnetic field range from −5 T to 5 T. The step-lengths of the applied magnetic field were set as 2 mT, 10 mT, 50 mT, 100 mT, and 500 mT in ranges up to 20 mT, 100 mT, 1000 mT, 2000 mT, and 5 T, respectively. The temperature dependence of the magnetic susceptibility was measured in the temperature range from 1.95–10 K in an applied magnetic field of $\mu_0 H = 20$ mT.

3. **Results and discussion**

3.1. *Compositions, structure, and thermal properties*

Each of the two glass series melted using the MQ and FC techniques comprised three samples with different Fe_2O_3 contents. All of the glasses were black in color and not transparent. Table 1 shows their nominal compositions and IDs. MQ and FC (IDs in Table 1) refer to the preparation methods and the numbers denote the

4

nominal Fe_2O_3 contents. SED-EDX measurements confirmed the compositions of the glasses and the presence of aluminum in all of the samples. The aluminum originated from the crucible material. The Al content was lowest at ~1 at% in glass FC15 and highest at ~5 at% in glass MQ15. The different Al contents determined for glasses with the same nominal composition can be attributed to the different melting times. The Al contents of the other samples were similar at ~2.5 at%. However, it should be noted that the SEM-EDX measurements were not sufficiently precise to determine the actual compositions of the inhomogeneous glasses. Iron-lead-silicate glasses are well known to contain different nanostructures [5], and thus the Al contents may have been overestimated or underestimated.

Table 1 Glasses and compositions. FC: fast-cooling method; MQ: melt-quenching technique.

Sample ID	Composition (mol%)	Composition (at%)
MQ12.5	$12.5Fe_2O_3$-$37.5PbO$-$50SiO_2$	$Fe_{8.7}Pb_{13}Si_{17.4}O_{60.9}$
MQ15	$15Fe_2O_3$-$35PbO$-$50SiO_2$	$Fe_{10.2}Pb_{11.9}Si_{16.9}O_{61}$
MQ17.5	$17.5Fe_2O_3$-$32.5PbO$-$50SiO_2$	$Fe_{11.6}Pb_{10.7}Si_{16.5}O_{61.2}$
FC12.5	$12.5Fe_2O_3$-$37.5PbO$-$50SiO_2$	$Fe_{8.7}Pb_{13}Si_{17.4}O_{60.9}$
FC15	$15Fe_2O_3$-$35PbO$-$50SiO_2$	$Fe_{10.2}Pb_{11.9}Si_{16.9}O_{61}$
FC17.5	$17.5Fe_2O_3$-$32.5PbO$-$50SiO_2$	$Fe_{11.6}Pb_{10.7}Si_{16.5}O_{61.2}$

Figure 1 shows the XRD curves obtained for all of the MQ samples (MQ12.5, MQ15, and MQ17.5) and FC sample FC17.5. Similar XRD results were obtained for the other FC samples (FC12.5 and FC15), so they are not presented in Fig. 1. The XRD curves obtained for all of the samples exhibited a typical glass bump, which is characteristic of amorphous materials.
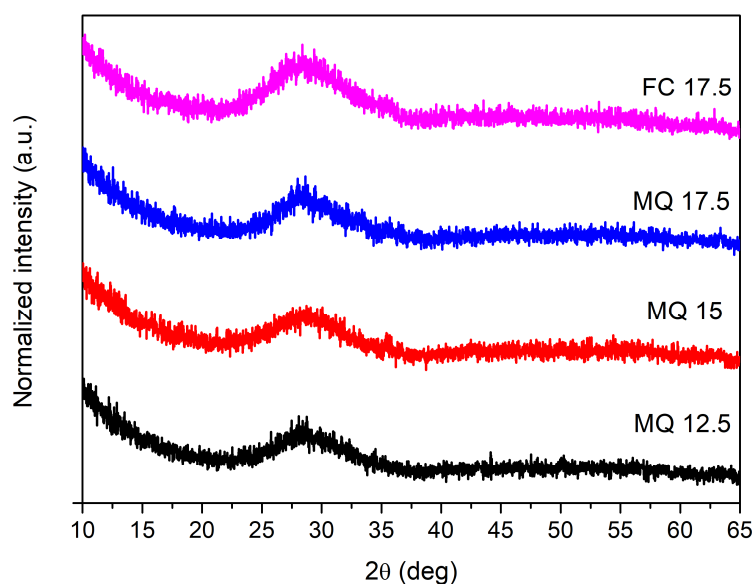
5

Figure 1. XRD curves obtained for all of the samples prepared using the melt-quenching technique (MQx) and for fast-cooled sample FC17.5.

SEM micrographs obtained from the fresh cross-sections of glasses MQ12.5, MQ15, and MQ17.5, and from the surfaces of glasses FC12.5, FC15, and FC17.5 are shown in Figs 2a–e. The topographic features of all the MQ glasses and FC15 and FC17.5 contained some inhomogeneities with sizes of less than 100 nm. The nanostructures visible in most of the glasses may have been formed from iron ions, which are known to locate in separate clusters measuring a few nanometers in iron-lead-silicate glasses [9, 16, 18]. Thus, the amount and size of the observed nanostructures were mainly dependent on the total iron content of the glass, so they were largest in MQ17.5 as a consequence. Moreover, the topographic features of the analogous glasses prepared by different techniques (MQx and FCx) differed greatly due to the impact of different cooling rates because the FCx glasses cooled approximately 10^5 times faster than the MQx glasses. The most obvious difference was between glasses MQ17.5 (Fig. 2c) and FC17.5 (Fig. 2f). FC17.5 contained only small evenly distributed nanostructures whereas MQ17.5 had additional large nanostructures, which were not evenly distributed. The results suggested that the longer cooling rate for the MQ glasses allowed iron ions to agglomerate into larger nanostructures and the bigger nanostructures were probably built from several smaller ones.

In the FCx glass series, sample FC12.5 (Fig. 2d) exhibited the characteristic topography of a homogenous glass with no evidence of any inhomogeneities. The

6

absence of inhomogeneities in this glass may have been due to the combined impact of the FC process, low Fe ion contents, and the presence of aluminum (~2.5 at%). Aluminum is known to form $[AlO_{4/2}]^-$ tetrahedra in many glasses [19-21] and it plays a clear intermediate glass-forming role. Moreover, the topography of glass FC12.5 (Fig. 2d) was homogenous at the micro-size scale, but it is possible that this glass contained small clusters that could not be observed with our SEM instrument.
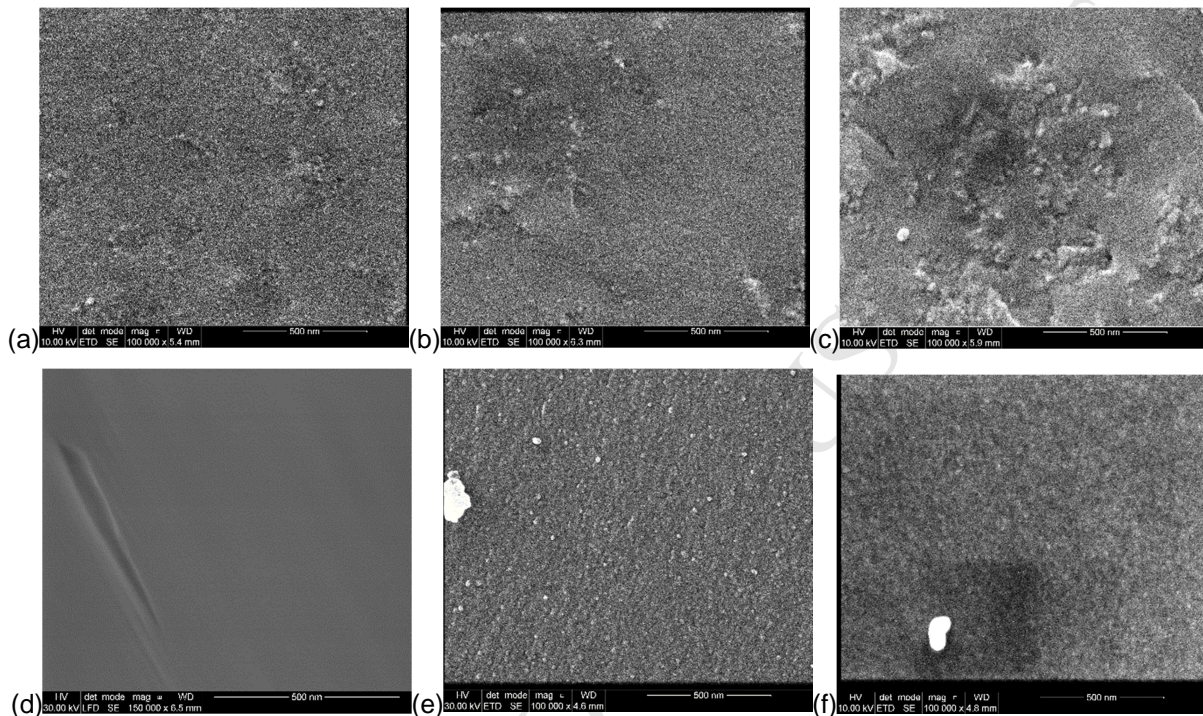

Figure 2. SEM micrographs for cross-sections of glasses: (a) MQ12.5, (b) MQ15, (c) MQ17.5 and surfaces of glasses: (d) FC12.5, (e) FC15 and (f) FC17.5 (for glass compositions see Table 1).

In our previous study [5], we synthesized samples with similar compositions (xFe$_2$O$_3$-50SiO$_2$-(50-x)PbO, where x = 15, 20, 25) and obtained multiphase structured glasses. We found that glass 15Fe$_2$O$_3$-35PbO-50SiO$_2$ contained spherical nanostructures measuring around 400 nm, which mostly comprised a Fe$_3$O$_4$ crystalline phase. However, the glasses obtained in the present study with analogous compositions were amorphous and the visible nanostructures were significantly smaller. The different topographic features of these glasses and the samples described in our previous study [5] were probably related to the different preparation conditions, particularly the crucible material (alumina crucibles) and the annealing process [5].

Table 2 shows the parameters of the thermal properties determined in experiments based on the DSC curves for all of the MQx and FCx glasses, i.e., the glass transition temperature $T_{g\ onset}$, exothermic process peak position $T_{exo1,\ peak}$

7

temperature, and the glass stability S. The glass stability describes the resistance to crystallization during heating and it was calculated as: $S = T_{exo1, peak} - T_{g\,onset}$ [22].

Table 2 Thermal properties of the series of MQx and FCx glasses, i.e., $T_{g\,onset}$ and $T_{exo1,\,peak}$ obtained from the DSC curves, and S.

| ID	$T_{g\,onset}$	$T_{exo1,\,peak}$	S
	(°C)	(°C)	(°C)
MQ12.5	536	860	324
MQ15	543	880	337
MQ17.5	539	870	331
FC12.5	552	850	298
FC15	529	820	291
FC17.5	530	820	290

The glass transition temperatures obtained for all of the glasses were similar and they varied between 529°C for FC15 and 552°C for FC12.5. First, we consider the T_g results obtained for the MQx glass series. T_g increased slightly for the glasses in the following order: MQ12.5 < MQ17.5 < MQ15, but the differences were not significant. Elements that participate in glass formation such as Al and Si [23] increase the T_g values of glasses, whereas the addition of a modifier oxide such as Pb typically decreases T_g. Iron ions may play a role as a network modifier at low contents and as a glass former at higher contents (>10 mol% of Fe_2O_3), thereby decreasing or increasing the glass-forming tendencies of glasses [24, 25]. Based on these assumptions, we can state that the highest T_g observed for MQ15 was probably due to its higher Al content (~5 at%) compared with the other MQx glasses (~2.5 at%). In addition, our comparison of the thermal properties of the glass FCx series showed that FC12.5 had a higher T_g value (for ~22°C) than FC15 and FC17.5. This may be explained by its more homogenous structure, where it was more polymerized than those with visible inhomogeneities. The effects of different Fe contents on the T_g values were not clear in the glasses investigated in this study.

The glass thermal stability values exhibited similar trends to T_g in the MQx and FCx glass series. However, the S values were lower for the FCx glasses than those estimated for the MQx samples. This difference was mainly due to the lower exothermic process temperatures for the FCx samples where the Fe ions were more evenly distributed in their glass structures. If we assume that the observed exothermic process was due to the crystallization process in the Fe-containing

8

phase, then we may state that the even distribution of Fe ions resulted in a lower temperature for the initiation of the crystallization process compared with those that had uneven distributions.
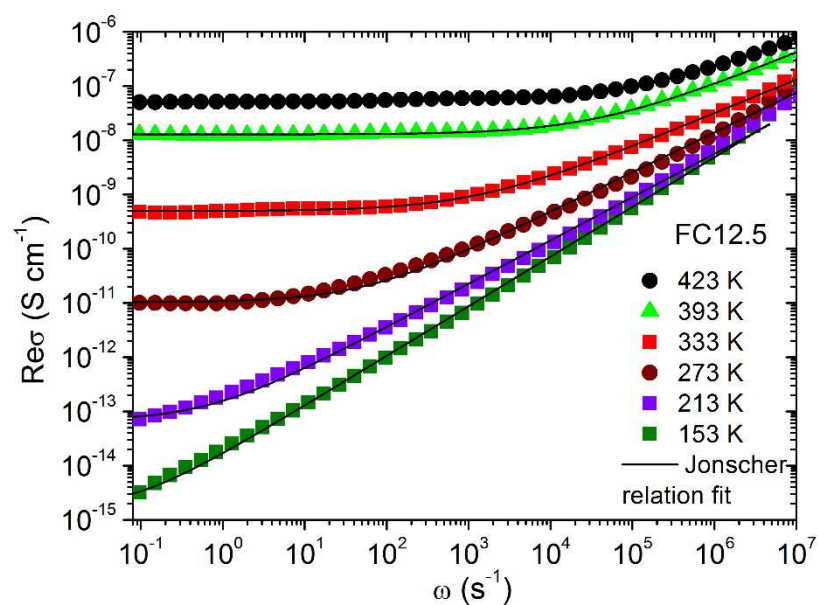
3.2. Electrical properties

Figures 3a–c show the real part of the conductivity as a function of the angular frequency at different temperatures for the samples prepared using different techniques (MQ12.5, MQ17.5, and FC12.5). All of the curves contained two regions, where the first was the DC plateau in the low angular frequency range and the second was the AC area of the curve for a high angular frequency range. For all of the compositions, the conductivity generally tended to increase as the temperature increased. There were significant differences in the conductivity behavior of all the MQ glasses. For MQ12.5 (Fig. 3a), the conductivity curve contained a distinct DC plateau region at temperatures ≥ 273 K and its frequency range reached up to six orders of magnitude at a temperature of 423 K. For MQ15 (not presented here) and MQ17.5 (Fig. 3b), the DC plateau was visible only at temperatures ≥ 333 K and the AC part was dominant at all of the temperatures measured. These changes in the conductivity behavior were not observed for the FC glasses. The conductivity curves obtained for FC15 and FC17.5 were similar to that for FC12.5 (Fig. 3c), and thus they are not shown.

(a)

9
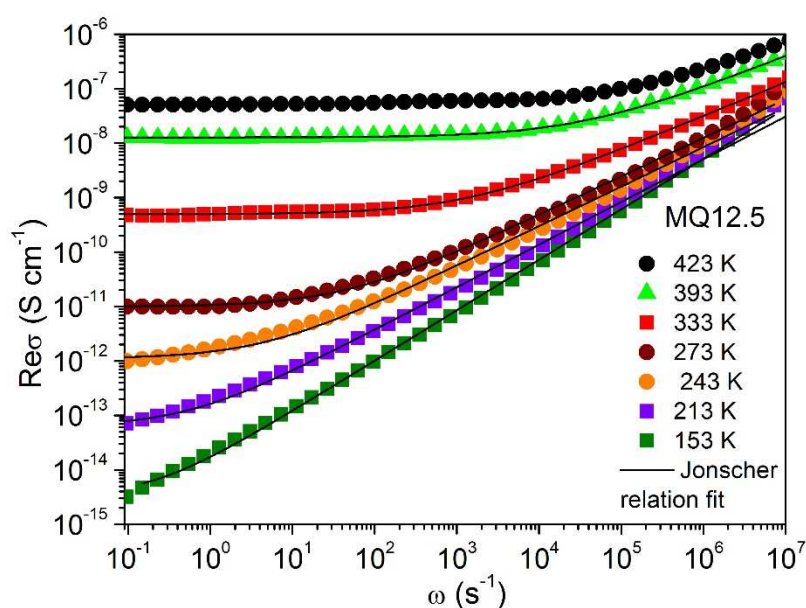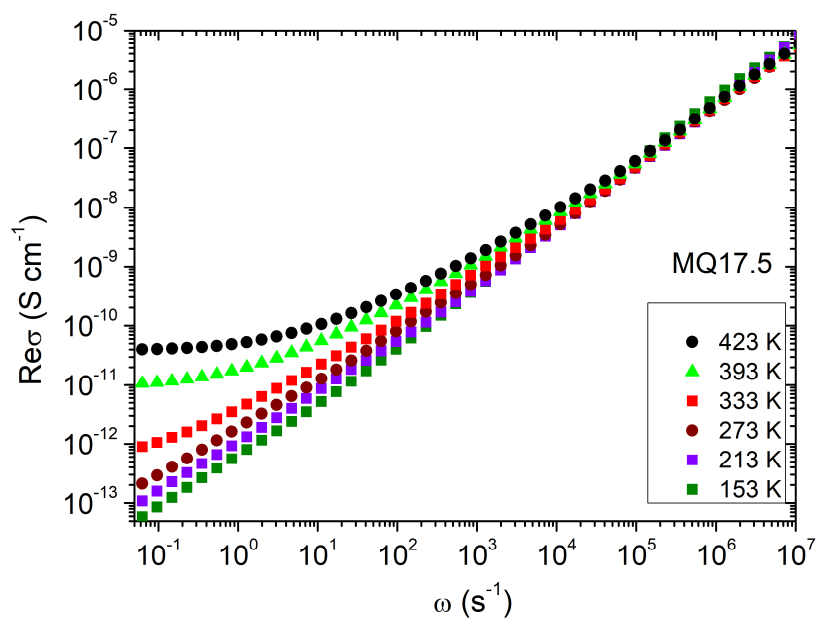
(b)

(c)

Figure 3. Real part of the conductivity as a function of the angular frequency measured at different temperatures for melt-quenched (MQ) glasses (a) MQ12.5 and (b) MQ17.5, and (c) fast-cooled glass FC12.5. The black lines are the fits obtained using Eq. 1.

The conductivity of many dielectric systems may be described by the Jonscher power law expressed by the relationship [26]:

$$\sigma'(\omega) = \sigma_{DC}(T) + A(T)\omega^{s(T)},\tag{1}$$

where $\sigma'(\omega)$ is the real part of total conductivity, σ_{DC} is the frequency-independent DC conductivity, and the coefficient A and exponent s ($0<s<1$) depend on the temperature and material properties. The term $A\omega^s$ contains the AC dependence and it characterizes the dispersion. Eq. (1) was fitted to the data obtained and the fitted results are shown by black lines in Fig. 3 for MQ12.5 and FC12.5. The DC conductivity values for all of the glasses are presented as a function of temperature in Fig. 4. The DC conductivity decreased in inverse proportion to the temperature for all of the glasses. The DC conductivity values measured at 393 K for all of the glasses are also listed in Table 3. Among the MQ glasses, the DC conductivity was highest for MQ12.5 and it was three orders of magnitude lower in MQ17.5 and MQ15. By contrast, in the FC samples, the DC conductivity was highest in FC17.5 and it was around two orders of magnitude lower in FC12.5 and FC15. In both series of glasses, the DC conductivity values were the same for the glasses containing 12.5 mol% Fe_2O_3 but the difference was five orders of magnitude between the MQ and FC glasses doped with 17.5 mol% Fe_2O_3. The DC conductivity in iron glasses is affected to a greater extent by the ratio of iron ions in two different valence states than by the total iron ion content. Moreover, the dispersion mode of the iron ions in the glass matrix is highly important. Therefore, in our glasses, the differences in the DC conductivities can be explained by the different sizes and dispersion modes of the iron-containing nanostructures, which created additional barriers to carrier hopping. The FCx glasses contained smaller nanostructures and they were evenly distributed in glass matrix, so the mean distance between the iron ions was approximately constant and the polaron hopping path was determined by the size of the sample. In the MQx glasses, the nanostructures agglomerated into larger inhomogeneities and they were unevenly distributed in the glass matrix, so the distances between iron ions located in neighboring inhomogeneities were longer and the hopping path was longer, thereby reducing the conductivity.
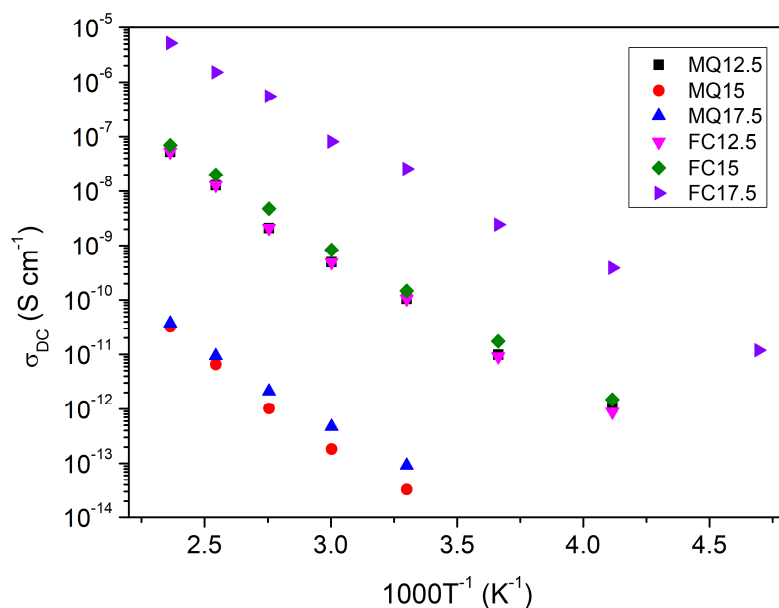
(a)
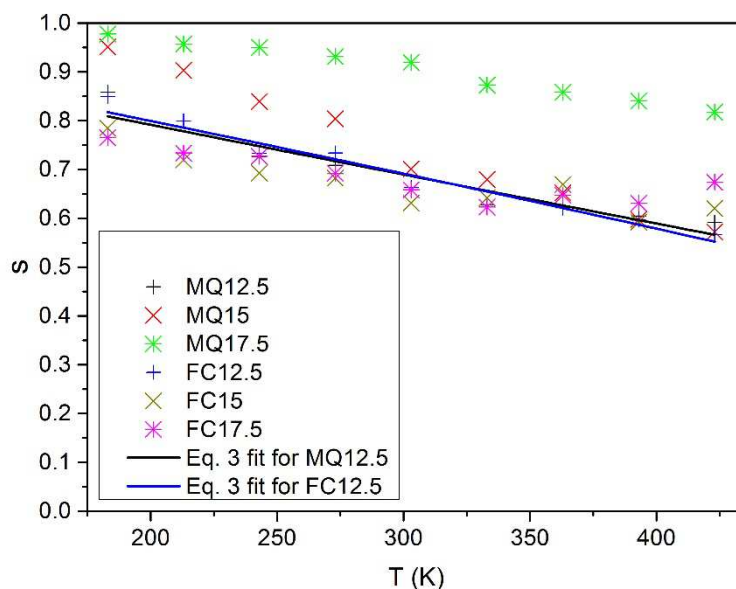
(b)

Figure 4. (a) DC conductivity as a function of 1000 T^{-1} for all of the glasses (estimated from Figs 3a–c) and (b) the parameter s as a function of temperature. The lines in (b) are the fits obtained using Eq. 3 for glasses MQ12.5 and FC12.5.

The change in the DC conductivity with temperature was not perfectly linear and it was found to change as predicted by Schnakenberg [27]. However, it was not possible to obtain satisfactory fits between our data and this model, probably due to the inhomogeneous structures of our samples, so we estimated the approximate activation energy values according to the Arrhenius equation:

$$\sigma_{DC}T = \sigma_0 exp\frac{-E_A}{k_BT}, \tag{2}$$

where σ_{DC} is the DC conductivity, σ_0 is a pre-exponential factor, k_B is the Boltzmann constant, E_A is the activation energy, and T is the temperature. The approximate activation energy values for the DC conductivity process are listed in Table 3, which shows that they ranged from 0.50 eV for FC17.5 to 0.67 eV for MQ15. These values are typical for the polaron hopping mechanism [13]. The lowest activation energy obtained for FC17.5 was in accordance with its highest DC conductivity compared with the other glasses. It should be noted that the FCx glass series had lower values for E_A and the thermal stability S (see Table 2) than MQx. High thermal stability is correlated with a low devitrification tendency, and thus the low mobility of polarons in glass.

Table 3. Sample IDs, DC conductivity measured at 393 K σ_{DC}, approximate activation energy values for the DC conductivity process E_A, and pre-exponential factor σ_0 estimated for all of the glasses.

ID	σ_{DC} (S cm^{-1}) at 393 K ± 5%		σ_0 (S cm^{-1} K) ± 5%		E_A (e) ± 5%	
	MQ	FC	MQ	FC	MQ	FC
MQ/FC12.5	$1.28 \cdot 10^{-8}$	$1.28 \cdot 10^{-8}$	55.2	72.8	0.55	0.56
MQ/FC15	$6.56 \cdot 10^{-12}$	$2.01 \cdot 10^{-8}$	0.9	100.2	0.67	0.56
MQ/FC17.5	$9.39 \cdot 10^{-12}$	$1.52 \cdot 10^{-6}$	0.1	1412.6	0.58	0.50

The pre-exponential factor σ_0 (from Eq. 1) for non-adiabatic polaron hopping may be obtained using the relationship described by Mott [14]: $\sigma_0 = C(1 - C)(e2u_{el}/RkT)exp(-2\alpha R)$, where C is the ratio of the concentration of Fe^{2+} ions relative to the total iron ion concentration ($C = [Fe^{2+}]/([Fe^{2+}] + [Fe^{3+}])$), R is the estimated distance between hopping centers, u_{el} is the electron frequency, and α is the wave function decay constant. The pre-exponential factor σ_0 may depend on the iron ion contents, valences, and dispersion mode in the glass matrix as well as the Fe ion environment. The values of σ_0 estimated (from Fig. 4 and Eq. 2) for the glasses are listed in Table 3. In the MQx glass series, the lowest values of the parameter σ_0 were determined for MQ15 and MQ17.5, which exhibited the lowest DC conductivity and the highest activation energy. The parameter σ_0 was significantly higher for MQ12.5, where the DC conductivity increased by three orders of magnitude. The σ_0 parameter values obtained for the FC glasses were higher than those for the MQ

samples. A significantly higher σ_0 parameter was determined for FC17.5, which agreed with its highest DC conductivity and lowest activation energy among all of the glasses.

ACCEPTED MANUSCRIPT

The results indicated that the preparation method significantly affected the electrical conductivity parameters. The FC glasses doped with ≥ 15% Fe_2O_3 had higher DC conductivity values than the MQ samples, possibly due to the more evenly distributed iron ions obtained from the FC process compared with those produced over a longer time in the MQ samples.

Elliott [15] determined the dependence of the exponent s from the Jonscher relationship (Eq. (1)) on the temperature in different conduction mechanisms in amorphous semiconductors. The values of the parameters estimated based on our experimental data are shown in Fig. 4b. In all of the samples, the exponent s decreased as the temperature increased. For most of the glasses, the exponent s decreased from about 0.8 to about 0.6. For MQ15, the maximum value of s was close to 0.95, whereas the s parameter decreased from about 1 to 0.85 for MQ17.5. Based on the values of s and its dependence on the temperature according to the models determined by Elliott, we suggest that the conduction process may have been due to overlapping polaron tunneling (OLP) in our glasses. The frequency exponent s for the OLP model can be evaluated as [15]:

$$s = 1 - \frac{4 + \frac{6W_{H0}r_0'}{kTR_\omega'^2}}{R_\omega'(1 + \frac{W_{H0}r_0'}{kTR_\omega'^2})^2}, \tag{3}$$

where $r_0' = 2\alpha r_0$ (r_0 is the polaron radius), α is the polarizability, $R_\omega' = 2\alpha R_\omega$, R_ω is the tunneling distance at a frequency ω, $W_H = W_{H0}(1 - r_0/R)$, W_H is the activation energy for polaron hopping, and W_{H0} is the reduced polaron hopping energy. The precise fitting of the OLP model to our data was not possible because of the inhomogeneous structure of our samples. However, the OLP model was fitted for samples MQ12.5 and FC12.5, and we obtained reasonable physical values: R_ω' =1.4 Å and R_ω' = 3.5 Å, and $W_{H0} \cdot r_0'$ = 0.7 eVÅ and $W_{H0} \cdot r_{0'}$ = 1.9 eVÅ, respectively. These results are only rough estimates, but they suggest that the reduced polaron radius and tunneling distance were lower for MQ12.5 than FC12.5.

3.3. Magnetic properties

14

The magnetic properties of the samples where iron was the only magnetic element were readily affected by small traces of the different Fe phases. Therefore, the magnetic hysteresis loops provided valuable information about the magnetic iron-containing phases [28]. The DC magnetization results normalized to the Fe content (see Tables 1 and 4) as a function of the magnetic field for the FC and MQ samples are shown in Fig. 5a and Fig. 5b, respectively. Both series of samples produced magnetic hysteresis loops. The hysteresis loops indicated that our samples were not fully saturated even at the highest applied field of 5 T [28]. The coercivity and remanence magnetization were estimated from Fig. 5 for all of the glasses, as shown in Table 4. It should be noted that the remanence and coercivity measurements may have been underestimated, and thus they are only approximate values.
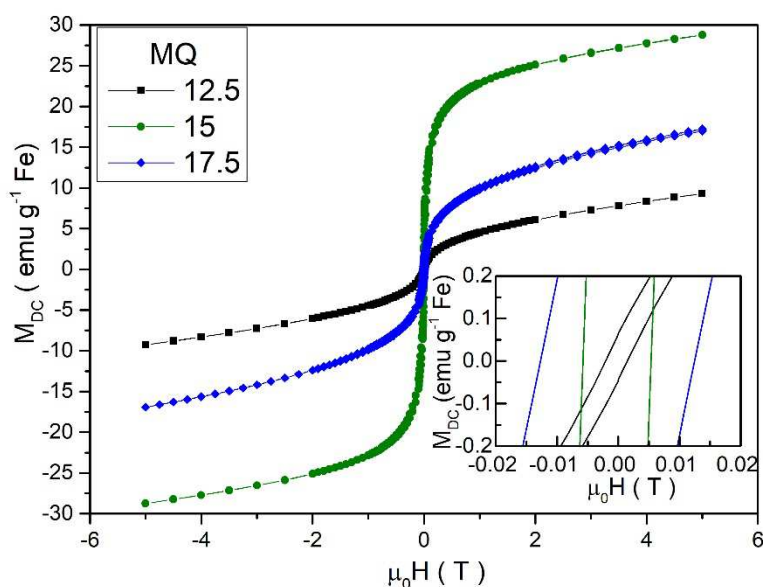
(a)
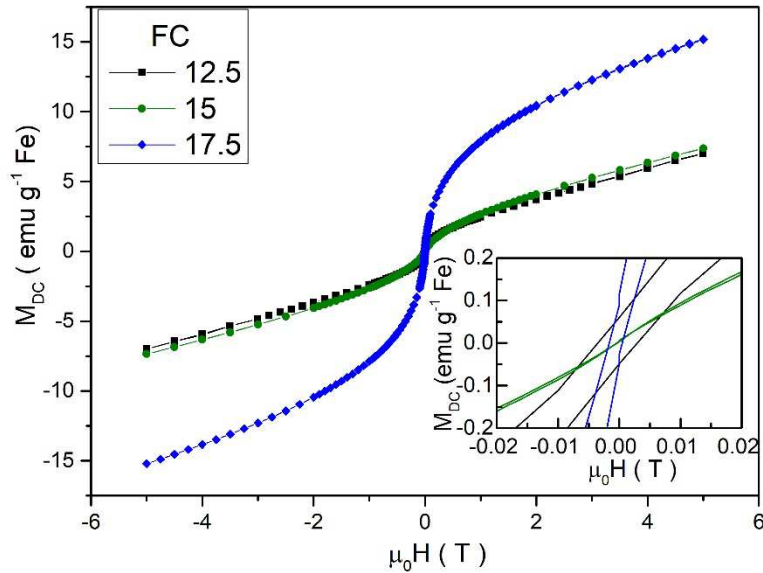
(b)

Figure 5. DC magnetization as a function of the magnetic field measured at 300 K for glasses prepared using: **(a)** the fast cooling (FC) and **(b)** melt quenching (MQ) techniques. Insets show the same plot expanded near the origin of the plot.

Table 4. Coercivity μ_0H_c and remanence magnetization M_R parameters for all glasses. FC: fast cooling method; MQ melt quenching technique.

| ID	μ_0H_c (mT)		M_R (emu/g Fe)	
	MQ	FC	MQ	FC
MQ/FC12.5	0.065	0.049	3.57	6.49
MQ/FC15	2.133	0.006	11.1	0.08
MQ/FC17.5	0.946	0.025	25.17	2.14

First, we consider the magnetic properties parameters obtained for the MQx glass series. The magnetic remanence increased for the glasses in the following order: 12.5 > 15 > 17.5, which agreed with the nominal Fe contents of these samples. The coercivity was highest for MQ15 and lower for MQ17.5 and MQ12.5. It is known that magnetite (Fe_3O_4), which is a ferrimagnetic phase, exhibits high magnetization and low coercivity, whereas canted antiferromagnetic hematite (α-Fe_2O_3) has low magnetization and high coercivity values. In addition, magnetite saturates magnetically at very low applied magnetic fields (<0.3 T) compared with hematite, and the coercivities depend greatly on the particle size, and thus the domain state [28]. Moreover, the coercivity parameter is influenced by the

16

concentration of structural defects. Therefore, the remanence magnetization and coercivity values estimated for the MQx glasses confirmed that the iron ion environments and distributions were different in the glass matrices. The majority of the iron ions probably formed magnetic and nonmagnetic phases located in the detected nanostructures (visible in the SEM micrographs), and thus the magnetic phase contents increased with the amount of added Fe_2O_3.

A significantly different situation was found in the FCx glass series, where the highest remanence magnetization was obtained for FC12.5 and the lowest for FC15. In addition, the coercivity was lowest for FC15. These findings suggest that the majority of the iron ions accumulated in the nanostructures, which were formed mostly by one of the nonmagnetic phases, probably FeO. This distribution of the Fe ions may explain the extremely low remanence magnetization and coercivity values calculated for the Fe ion (see Table 4).

A more detailed comparison of the composition of the glasses demonstrated that those prepared using the FC method had narrower magnetic hysteresis loops than those prepared with the traditional MQ technique, probably because of the lack of sufficient time to achieve structure reordering and relaxation in the FC samples. In these glasses, the magnetic domains were smaller or they lacked domains, and thus anchoring of the magnetic field was not observed. The magnetization in the glasses was middle magnetic hard and it depended on the iron content, but mostly on the iron ion distribution and clustering process, which were fixed during the cooling process.

17
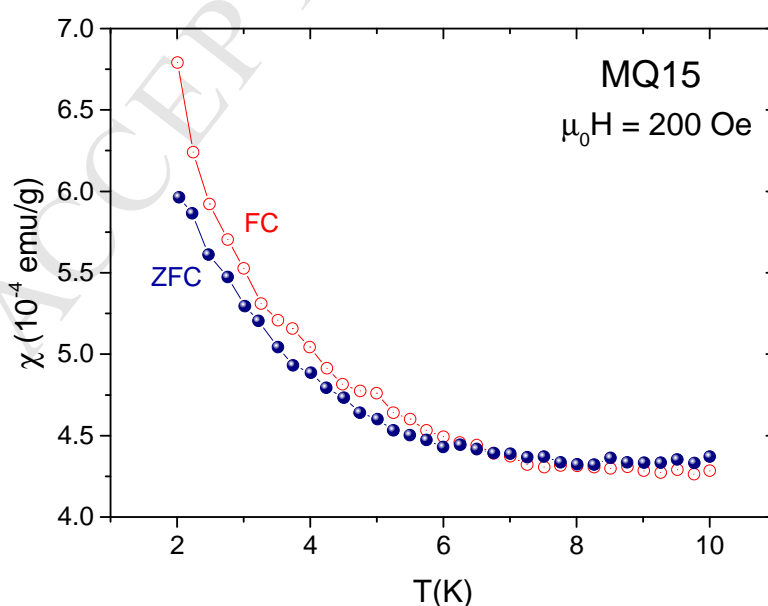
The thermal zero field cooled and field cooled magnetizations were measured for all of the glasses to determine their possible spin glass transition temperatures. The temperature dependence of the DC magnetic susceptibility χ(T) at μ$_0$H = 20 mT for glass MQ15 is presented in Fig. 6. Only a small difference was observed between the zero field cooled and field cooled plots, thereby suggesting that a spin-glass transition was not present in the sample down to 1.9 K. Frustration of the magnetic interactions is necessary for spin-glass behavior to occur [29-42]. This type of behavior was unlikely to occur in our system because of the ferromagnetic interactions between the iron atoms. The results obtained for the other samples were analogous to those for MQ15.

4. **Conclusions**

In this study, samples with composition of xFe_2O_3-(50-x)PbO-50SiO_2, where x = 12.5, 15, and 17.5, were prepared using MQ and FC methods. All of the glasses were found to be amorphous and nanostructures with a mean size less than 100 nm were observed in most. The detected nanostructures were larger in the MQ samples and their distribution was more even in FC samples.

The thermal properties showed that the glass transition temperature T_g was similar for all of the glasses and it varied between 529°C and 552°C. The thermal stability was lower for the FC glasses than the MQ glasses, mainly because of the more even distribution of Fe ions in the structures of the FC glasses.

The AC and DC conductivity were measured for the glasses using the impedance spectroscopy method. The mechanism of the DC conduction process was attributed to polaron hopping in all of the glasses. The FC glasses had higher values for the DC conductivity and pre-exponent σ_0 but lower activation energies than the MQ glasses, probably because of the smaller distance for hopping between the evenly distributed iron ions and thus a longer conduction path compared with the unevenly distributed larger iron-containing inhomogeneities.

The magnetization was measured as a function of the magnetic field and magnetic hysteresis was observed in all of the glasses. The FC glasses had lower coercivity values than the MQ glasses because of their smaller magnetic domains or a lack of them.

18

References

[1] I. Ardelean, G. Ilonca, M. Peteanu, D. Pop, Magnetic properties of xMnO(1-x) [19TeO$_2$PbO] glasses, Solid State Communications 3 (1980) 653–655.

[2] C. H. Perry, D. L. Kinser, L. K. Wilson, J. G. Vaughn, Magnetic exchange between Ti^{3+} ions in titanium phosphate glass, Journal of Applied Physics 50 (1979) 1601–1603.

[3] E. J. Freibele, N. C. Koon, Magnetization studies of amorphous antiferromagnetism in manganase phosphate glass, Solid State Communications 14 (1974) 1247–1250.

[4] E. J. Freibele, N. C. Koon, L. K. Wilson, D. L. Kinser, Magnetic properties of an amorphous antiferromagnet, Journal of the American Ceramic Society 57 (1974) 237.

[5] R. J. Barczyński, N. A. Szreder, J. Karczewski, M. Gazda, Electronic conductivity in the SiO$_2$–PbO–Fe$_2$O$_3$ glass containing magnetic nanostructures, Solid State Ionics 262 (2014) 801–805.

[6] D. Yousefi, M. Tavoosi, A. Ghasemi, Magnetic properties of B$_2$O$_3$-SiO$_2$-BaO-Fe$_2$O$_3$ glass-ceramics, Journal of Non-Crystalline Solids 443 (2016) 1–7.

[7] O. H. El-Bayoumi, R. K. MacCrone, Dielectric behavior of lead-silicate glasses containing iron, Journal of the American Ceramic Society 59 (1976) (9–10) 386–392.

[8] D. W. Moon, J. M. Aitken, R. K. MacCrone, Magnetic properties and structure of xFe$_2$O$_3$ (1-x)[BaO-4B$_2$O$_3$] glasses, Physics and Chemistry of Glasses 16 (1975) (5) 91–102.

[9] K. J. Kim, M. P. Maley, R. K. MacCrone, in: R. A. Levy, Hasegawa (Eds.), Electronic conductivity in the SiO$_2$–PbO–Fe$_2$O$_3$ glass containing magnetic nanostructures, Plenum Press, New York, Amorphous Magnetism Vol. II (1977) 627.

[10] S. K. Mendiratta, M. A. Valente, J. A. Perenboom, Magnetization behaviour of Gd lead borate and Fe lead borate glasses under high magnetic field 20 T, Journal of Non-Crystalline Solids 134 (1990) 100–106.

[11] L. Murawski, Review Electrical conductivity in iron-containing oxide glasses, Journal of Materials Science 17 (1982) 2155–2163.

[12] L. Živanov, M. Damnjanović, N. Blaž, A. Marić, M. Kisić, G. Radosavljević, Soft ferrite applications, Magnetic, Ferroelectric, and Multiferroic Metal Oxides (2018) 387–409, doi:10.1016/B978-0-12-811180-2.00019-0.

[13] L. Murawski, R. J. Barczyński, Dielectric properties of transition metal oxide glasses, Journal of Non-Crystalline Solids 185 (1995) 84–93.

[14] N. F. Mott, Conduction in glasses containing transition metal ions, Journal of Non-Crystalline Solids 1 (1968) 1–17.

[15] R. S. Elliot, AC conduction in amorphous chalcogenide and pnictide semiconductors, Advances in Physics 36 (2) (1987) 135–218.

[16] R. A. Anderson, R. K. MacCrone, Electronic relaxation in the PbO-SiO_2-Fe_2O_3 glass system, Journal of Non-Crystalline Solids 14 (1974) 112–130.

[17] A. Amzil, R. Castanet, Thermodynamic Investigation of the Pt-Pb binary alloys, Berichte der Bunsengesellschaft für physikalische Chemie 96 (12) (1992) 1872–1876, doi:10.1002/bbpc.19920961217.

[18] M. Fahmy, M. J. Park, M. Tomozawa, R. K. MacCrone, Magnetic properties, microstructure, and ultrastructure of partially crystallized B2O3-BAO-FE2O3 glass, Phys. Chem. Glasses 13 (1972) 2.

[19] E. Morin, J. Wu, J. Stebbins, Modifier cation (Ba, Ca, La, Y) field strength effects on aluminum and boron coordination in aluminoborosilicate glasses: the roles of fictive temperature and boron content, Applied Physics A 116 (2014) 479–490, 10.1007/s00339-014-8369-4.

[20] C. Le Losq, D. R. Neuville, P. Florian, G. S. Henderson, D. Massiot, The role of Al^{3+} on rheology and structural changes in sodium silicate and aluminosilicate glasses and melts, Geochimica Cosmochimica Acta 126 (2014) 495–517, doi:10.1016/j.gca.2013.11.010.

[21] L. M. Thompson, J. F. Stebbins, Non-stoichiometric non-bridging oxygens and five-coordinated aluminum in alkaline earth aluminosilicate glasses: Effect of modifier cation size, Journal of Non-Crystalline Solids 358 (2012) 1783–1789, doi:10.1016/j.jnoncrysol.2012.05.022.

[22] V. Simon, D. Muresan, A. Takacs, M. Neumann, S. Simon, Local order changes induced in calcium–sodium–phosphate glasses by transition metals, Solid State Ionics 178 (2007) 221–225, doi:10.1016/j.ssi.2006.12.011.

[23] S. G. Griffin, R. G. Hill, Influence of glass composition on the properties of glass polyalkenoate cements. Part II: influence of phosphate content, Biomaterials 21 (2000) 399–403.

[24] R. Parmar, R. S. Kundu, R. Punia, P. Aghamkar, N. Kishore, Effect of Fe_2O_3 on the physical and structural properties of bismuth silicate glasses, AIP Conf. Proc. 1536, 653 (2013), doi:10.1063/1.4810396.

[25] D. Aboutaleb, B. Safi, Structure and properties of the soda-borate glasses: effect of adding Fe_2O_3 concentration, Journal of Chemical Engineering Process Technology 2016, 7:1, doi:10.4172/2157-7048.1000268.

[26] A. K. Jonscher, Dielectric Relaxation in Solids, Chelsea Dielectrics Press London 1983, ISBN 0 9508711 0 9.

[27] J. Schnakenberg, Polaronic impurity hopping conduction, Phys. State. Solids 28, 623 (1968).

[28] M. Ahmadzadeh, J. Marcial, J. McCloy, Crystallization of iron-containing sodium aluminosilicate glasses in the $NaAlSiO_4$-$NaFeSiO_4$ join, Journal of Geophysical Research: Solid Earth 122 (2017) 2504–2524, doi:10.1002/2016JB013661.

[29] A. P. Ramirez, Strongly geometrically frustrated magnets, Annual Review of Materials Science 24 (1994) 453–480, doi:10.1146/annurev.ms.24.080194.002321.

[30] H. El. Moussaoui, T. Mahfoud, S. Habouti, K. El. Maalam, M. Ben Ali, M. Hamedoun, O. Mounkachi, R. Masrour, E. K. Hlil, A. Benyoussef, Synthesis and magnetic properties of tin spinel ferrites doped manganese, Journal of Magnetism and Magnetic Materials 405 (2016) 181–186, doi:10.1016/j.jmmm.2015.12.059.

[31] O. Mounkachi, M. Hamedoun, M. Belaiche, A. Benyoussef, R. Masrour, H. El. Moussaoui, M. Sajieddine, Synthesis and magnetic properties of ferrites spinels $Mg_xCu_{1-x}Fe_2O_4$, Physica B 407 (1) (2012) 27–32, doi:10.1016/j.physb.2011.09.023.

[32] M. Ben Ali, K. El. Maalam, H. El. Moussaoui, O. Mounkachi, M. Hamedoun, R. Masrour, E. K. Hlil, A. Benyoussef, Effect of zinc concentration on the structural and magnetic properties of mixed Co–Zn ferrites nanoparticles synthesized by sol/gel method, Journal of Magnetism and Magnetic Materials 398 (2016) 20–25, doi:10.1016/j.jmmm.2015.08.097.

[33] R. Masrour, E. K. Hlil, S. Obbade, C. Rossignol, Theoretical and experimental investigations of the structural, magnetic, electronic, and electrical properties of olivine $LiFePO_4$, Solid State Ionics 289 (2016) 214–219, doi:10.1016/j.ssi.2016.03.016.

[34] O. Mounkachi, H. El Moussaoui, R. Masrour, J. Ilali, K. El. Mediouri, M. Hamedoun, E.K. Hlil, A. El Kenzb, A. Benyoussef, High freezing temperature in SnO_2 based diluted magnetic semiconductor, Materials Letters 126 (2014) 193–196, doi:10.1016/j.matlet.2014.04.064.

[35] R. Masrour, A. Jabar, H. Khlif, F. Ben Jemaa, M. Ellouze, E. K. Hlil, Experiment, mean field theory and Monte Carlo simulations of the magnetocaloric effect in

$La_{0.67}Ba_{0.22}Sr_{0.11}MnO_3$ compound, Solid State Communications 268 (2017) 64–69, doi:10.1016/j.ssc.2017.10.003.

[36] K. El Maalam, M. Ben Ali, H. El Moussaoui, O. Mounkachi, M. Hamedoun, R. Masrour, E. K. Hlil, A. Benyoussef, Magnetic properties of tin ferrites nanostructures doped with transition metal, Journal of Alloys and Compounds 622 (2015) 761–764, doi:10.1016/j.jallcom.2014.10.152.

[37] H. El Moussaoui, O. Mounkachi, R. Masrour, M. Hamedoun, E. K. Hlil, A. Benyoussef, Synthesis and super-paramagnetic properties of neodymium ferrites nanorods, Journal of Alloys and Compounds 581 (2013) 776–781, doi:10.1016/j.jallcom.2013.07.139.

[38] H. El Moussaou, T. Mahfoud, M. Ben Ali, Z. Mahhouti, R. Masrour, M. Hamedoun, E. K. Hlil, A. Benyoussef, Experimental studies of neodymium ferrites doped with three different transition metals, Materials Letters 171 (2016) 142–145, doi:10.1016/j.matlet.2016.02.072.

[39] O. Mounkachi, E. Salmani, H. El Moussaoui, R. Masrour, M. Hamedoun, H. Ez-Zahraouy, E. K. Hlil, A. Benyoussef, High blocking temperature in SnO_2 based super-paramagnetic diluted magnetic semiconductor, Journal of Alloys and Compounds 614 (2014) 401–407, doi:10.1016/j.jallcom.2014.06.028.

[40] M. Ben Ali, O. Mounkachi, K. El Maalam, H. El Moussaoui, M. Hamedoun, E. K. Hlil, D. Fruchart, R. Masrour, A. Benyoussef, Coexistence of blocked, metamagnetic and canted ferrimagnetic phases at high temperature in Co–Nd ferrite nanorods, Superlattices and Microstructures 84 (2015) 165–169, doi:10.1016/j.spmi.2015.05.002.

[41] R. Masrour, M. Hamedoun, A. Benyoussef, E. K. Hlil, Magnetic properties of mixed Ni–Cu ferrites calculated using mean field approach, Journal of Magnetism and Magnetic Materials 363 (2014) 1–5, doi:10.1016/j.jmmm.2014.03.043.

[42] R. Masrour, M. Hamedoun, A. Benyoussef, The magnetic properties of oxide spinel $Li_{0.5}Fe_{2.5-2x}Al_xCr_xO_4$ solid solutions, Physica B 407 (7) (2012) 1161–1165, doi:10.1016/j.physb.2012.01.106.

22

Iron-lead-silicate glasses prepared by melt quenching (MQ) and fast cooling (FC).

MQ glasses had larger and more unevenly distributed nanostructures than FC ones.

Glass transition temperatures similar for all glasses at around 540°C.

FC glasses had higher DC conductivity values and lower activation energies.

FC glasses had lower coercivity values than MQ glasses.